AGU PUBLICATIONS

JGR

Journal of Geophysical Research: Biogeosciences

RESEARCH ARTICLE
10.1002/2015JG002965

Key Points:
- Large fires became more significant in the U.S. over recent decades
- Larger fires were associated with higher burn severity
- Fire emission model can be improved by coupling remote-sensed burn severity

Supporting Information:
- Supporting Information S1

Correspondence to:
H. Tian,
tianhan@auburn.edu

Citation:
Yang, J., H. Tian, B. Tao, W. Ren, S. Pan, Y. Liu, and Y. Wang (2015), A growing importance of large fires in conterminous United States during 1984–2012, *J. Geophys. Res. Biogeosci., 120*, 2625–2640, doi:10.1002/2015JG002965.

Received 18 FEB 2015
Accepted 30 NOV 2015
Accepted article online 11 DEC 2015
Published online 30 DEC 2015

A growing importance of large fires in conterminous United States during 1984–2012

Jia Yang[1], Hanqin Tian[1], Bo Tao[1,2], Wei Ren[1,2], Shufen Pan[1], Yongqiang Liu[3], and Yuhang Wang[4]

[1]International Center for Climate and Global Change Research, School of Forestry and Wildlife Sciences, Auburn University, Auburn, Alabama, USA, [2]Department of Plant and Soil Sciences, College of Agriculture, Food, and Environment, University of Kentucky, Lexington, Kentucky, USA, [3]Center for Forest Disturbance Science, USDA Forest Service, Athens, Georgia, USA, [4]School of Earth and Atmospheric Sciences, Georgia Institute of Technology, Atlanta, Georgia, USA

Abstract Fire frequency, extent, and size exhibit a strong linkage with climate conditions and play a vital role in the climate system. Previous studies have shown that the frequency of large fires in the western United States increased significantly since the mid-1980s due to climate warming and frequent droughts. However, less work has been conducted to examine burned area and fire emissions of large fires at a national scale, and the underlying mechanisms accounting for the increases in the frequency of large fires are far from clear. In this study, we integrated remote-sensed fire perimeter and burn severity data sets into the Dynamic Land Ecosystem Model to estimate carbon emissions from large fires (i.e., fires with size larger than 1000 acres or 4.05 km^2) in conterminous United States from 1984 to 2012. The results show that average area burned by large fires was 1.44×10^4 km^2 yr^{-1} and carbon emissions from large fires were 17.65 Tg C yr^{-1} during the study period. According to the Mann-Kendall trend test, annual burned area and pyrogenic carbon emissions presented significant upward trends at the rates of 810 km^2 yr^{-1} and 0.87 Tg C yr^{-1}, respectively. Characteristic fire size (fire size with the largest contribution to the total burned area) in the period of 2004–2012 increased by 176.1% compared to the period of 1984–1993. We further found that the larger fires were associated with higher burn severity and occurred more frequently in the warmer and drier conditions. This finding implies that the continued warming and drying trends in the 21st century would enhance the total burned area and fire emissions due to the contributions of larger and more severe wildfires.

1. Introduction

As a natural disturbance in the Earth system, fire plays a critical role in climate changes [*Bowman et al.*, 2009; *Randerson et al.*, 2006; *Ward et al.*, 2012] by modifying vegetation composition and distribution [*Bond et al.*, 2005], greenhouse gases and aerosol concentrations [*Bousquet et al.*, 2006; *Kasischke et al.*, 2005; *Langmann et al.*, 2009; *van der Werf et al.*, 2004], the terrestrial carbon budget [*Bond-Lamberty et al.*, 2007; *Houghton et al.*, 2000; *Li et al.*, 2014; *Prentice et al.*, 2011; *Yang et al.*, 2015], and land surface water and energy balance [*Beck et al.*, 2011; *Bond-Lamberty et al.*, 2009]. In conterminous United States (CONUS), wildfires have been intensively studied at various temporal and spatial scales [e.g., *Houghton et al.*, 2000; *Liu*, 2004; *Schoennagel et al.*, 2004; *Westerling et al.*, 2006; *Zhang et al.*, 2014]. It was reported that burned area in CONUS declined by 98% from the 1700s to the late twentieth century mainly due to human activities (i.e., fire suppression, grazing, and cropland expansion) [*Houghton et al.*, 2000]. However, since the mid-1980s, the frequency of wildfires in the western U.S. increased substantially owing to the elevated temperature, earlier spring, and more frequent droughts [*Dennison et al.*, 2014; *Littell et al.*, 2009; *Westerling et al.*, 2006].

Large fires accounted for a majority of the total burned area despite comprising only a small fraction of total fires [*Urbanski et al.*, 2011; *Barbero et al.*, 2014; *North et al.*, 2015]. Satellite observations showed that the frequency of large fires in the western U.S. presented an increasing trend in recent decades [*Barbero et al.*, 2014; *Dennison et al.*, 2014], which substantially modified the pattern of energy, water, and carbon exchanges between land and the atmosphere [e.g., *Dore et al.*, 2012]. Previous studies put emphasis on fire frequency, burned area, and fire emissions [e.g., *Urbanski et al.*, 2011], while relatively less effort was devoted to studying the temporal changes in fire size and burn severity of large fires at a national level in the United States.

To investigate the changes of fire size from 1959 to 1999 in boreal North America, *Kasischke and Turetsky* [2006] analyzed the frequency and burned area of fires in four size categories (i.e., small, large, very large, and ultra large) and found a significant increase in the frequency of large fires in the 1980s and the 1990s,

comparing with the 1960s and the 1970s. *Barbero et al*. [2014] found an increase in the probability of very large fires (>5000 ha) in the western U.S. from 1984 to 2010 based on a statistical model. *Lehsten et al*. [2014] developed the concept of "characteristic fire size" to describe the relative contribution of fires in different size categories to the total burned area and investigated the spatial distribution and temporal variation of fire sizes across the boreal ecoregions. However, the changes in fire size in CONUS have not been well studied and need to be examined urgently.

The term "burn severity" is generally used to describe the magnitude of aboveground and belowground organic matter consumed by fires [*Keeley*, 2009]. Fires with different levels of burn severity can induce divergent ecological consequences [*Schoennagel et al*., 2004]; low-severity fires usually do not kill trees and produce less fire emissions, while high-severity fires are either very hot surface fires or crown fires and often kill trees and alter vegetation composition. Larger and more severe fires produce higher fire emissions, generate a higher risk of soil erosion, and slow down postfire plant recovery. At the landscape level, biomass consumption was found to be determined by weather conditions, fuel characteristics, and topography [*Dillon et al*., 2011]. However, a general relationship between burn severity and fire size has not been demonstrated at a national scale.

The emissions of gases and particulates from fires are one major pathway through which fires influence atmospheric greenhouse gas concentrations and air quality. Currently, two primary approaches are used to estimate pyrogenic carbon emissions, i.e., satellite-based approach and fire emission modeling. Basically, satellite-based approach estimates pyrogenic carbon emissions based on fire radiative power (FRP) and biomass combustion rate [*Kaiser et al*., 2012; *Wooster et al*., 2005; *Zhang et al*., 2014], while fire models estimate pyrogenic carbon emissions based on burned area, fuel loading, and combustion completeness [*Seiler and Crutzen*, 1980]. Burned area can either be obtained from input data sets [e.g., *van der Werf et al*., 2010] or from model simulations [e.g., *Li et al*., 2012]. Input burned area data sets employed in most fire models are from satellite-based observations [e.g., *van der Werf et al*., 2010; *Wiedinmyer et al*., 2011; *Urbanski et al*., 2011; *French et al*., 2014]. The representation of combustion completeness and tree mortality in fire emission models can either be retrieved from a fixed vegetation parameter table [e.g., *Li et al*., 2012; *Thonicke et al*., 2010] or be simulated according to fuel characteristics and meteorological conditions [e.g., *French et al*., 2014; *Urbanski et al*., 2011; *Larkin et al*., 2014; *Veraverbeke et al*., 2015].

In the U.S., national-scale remote-sensed fire perimeter and burn severity have been developed by the Monitoring Trends in Burn Severity (MTBS) project [*Eidenshink et al*., 2007] and applied to estimate fire emissions and forest mortality across various landscapes and regions [*Dennison et al*., 2014; *Dillon et al*., 2011; *Ghimire et al*., 2012; *Hicke et al*., 2013; *Meigs et al*., 2011; *Miller et al*., 2012]. The MTBS fire products mapped fire perimeters and burn severity of large fires with size over 1000 acres (4.05 km^2) in the western U.S. and size over 500 acres (2.02 km^2) in the eastern U.S. In this study, we examined fire size, burned area, and burn severity in CONUS by using the spatially explicit MTBS fire products spanning from 1984 to 2012. Then, we incorporated the MTBS fire products into a process-based ecosystem model, the Dynamic Land Ecosystem Model (DLEM) [*Tian et al*., 2010a], to estimate fire-induced carbon emissions by considering temporal and spatial variations of remote-sensed burn severity. The specific objectives of this study are the following: (1) to investigate the changing trends of fire size and burned area in CONUS, (2) to provide a new estimation of pyrogenic carbon emissions in CONUS by coupling remote-sensed burn severity, and (3) to probe the relationship between fire size and burn severity.

2. Method and Data

2.1. Data Sets

2.1.1. Climate Data Sets and Indices

In this study, climate data from 1979 to 2012 were obtained from North American Regional Reanalysis (NARR) data set at the spatial resolution of 32 km [*Mesinger et al*., 2006] (available at http://www.esrl.noaa.gov/psd/data/gridded/data.narr.monolevel.html). We interpolated the NARR climate product to the geographic coordinate system at 0.25° resolution by using ArcInfo 10.0. The *z* scores of annual temperature and precipitation (T_z and P_z) were computed to represent the year-to-year climate variations from 1984 to 2012,

$$T_z = \frac{T - \overline{T}}{\sigma_T} \tag{1a}$$

$$P_z = \frac{P - \overline{P}}{\sigma_P} \tag{1b}$$

where T is the annual mean temperature (°C), $\overline{T}$ is the 29 year average annual mean temperature (°C), σ_T is the standard deviation of 29 year annual temperature (°C), P is the annual total precipitation (mm yr^{-1}), $\overline{P}$ is the 29 year average precipitation (mm yr^{-1}), and σ_P is the standard deviation of 29 year annual precipitation (mm yr^{-1}).

2.1.2. MTBS Fire Database

The MTBS is a multiyear project designed to consistently map the burn severity and perimeters of fire across all the lands of the United States from 1984 and beyond (http://www.mtbs.gov/). The satellite-based burned severity index, i.e., differenced normalized burn ratio (dNBR), was used to retrieve fire perimeters and burn severity [*Eidenshink et al*., 2007]. The dNBR compared well with ground-based composite burn index (CBI) in CONUS [*Cocke et al*., 2005; *Key and Benson*, 2006; *Miller and Thode*, 2007; *Veraverbeke et al*., 2011] and has been recognized as an effective approach to map burn severity [*Brewer et al*., 2005]. Based on the relationship between dNBR and CBI, satellite pixels within fire perimeter were classified into four severity levels, namely, "unburn to low," "low," "medium," and "high." Negative dNBR indicates increased photosynthesis activities of postfire vegetation, and therefore, pixels with negative dNBR were classified as "increased greenness" in the MTBS. We grouped these pixels into the severity level of unburn to low. Pixels labeled by "nonprocessing area mask" refer to pixels within the gaps between satellite imaging swaths or the pixels contaminated by cloud. MTBS burn severity was provided in the raster format at the spatial resolution of 30 m, and fire perimeters were provided in the format of ArcGIS shapefile (see the example of the "North Fork" fire in Figure S1 in the supporting information). In this study, we used the area within fire perimeter to denote burned area, which could be slightly larger than the actual area burned owing to the existence of unburnt vegetation islands (see the uncertainties in section 3.5).

The MTBS project includes fires larger than 1000 acres (4.05 km^2) in the western U.S. (west of 97°W longitude) and fires larger than 500 acres (2.02 km^2) in the eastern U.S. (east of 97°W longitude) [*Eidenshink et al*., 2007]. In this study, we only investigated the emissions and burn severity of large fires (>1000 acres) and excluded fires less than 1000 acres in size. In total, 14,495 large fires during 1984–2012 were included in this study (Figure 1). We further separated these fires into three size categories: large (L), very large (VL), and ultralarge (UL), based on the fire size (in acre) as below

$$\text{Category L:} \quad 3 \le \log_{10}(\text{fire size}) < 4$$
$$\text{Category VL:} \quad 4 \le \log_{10}(\text{fire size}) < 5$$
$$\text{Category UL:} \quad \log_{10}(\text{fire size}) \ge 5$$

The statistics of fire count and average burned area in each size category are shown in Table S1. We extracted monthly fire perimeters and burn severity according to fire starting dates and locations. Burn severity of one specific fire event was represented by the fractions of fire pixels in different severity levels. For example, in the North Fork fire (Figure S1), 869,025 pixels (34.2%) were burned in unburn to low severity; 167,398 pixels (6.6%) were burned in low severity; 294,284 pixels (11.6%) were burned in "Moderate" severity; 1,150,086 pixels (45.3%) were burned in high severity; increased greenness took 52,283 pixels (2.1%); and nonprocessing area mask took 7781 pixels (0.3%).

2.2. The Dynamic Land Ecosystem Model (DLEM)

The DLEM is a highly integrated, process-based land ecosystem model, which simulates the water, energy, and biochemical cycles between terrestrial ecosystem and atmosphere under the impacts of multiple environmental factors, including climate, ambient CO_2, nitrogen deposition, land use/land cover change, and fire disturbances [*Pan et al*., 2014; *Ren et al*., 2012; *Tian et al*., 2010a, 2010b, 2012]. The DLEM consists of five core components: (1) biophysics, (2) plant physiology, (3) soil biogeochemistry, (4) dynamic vegetation, and (5) land use, disturbance, and land management. Recently, we improved the DLEM by coupling the river routing, water quality, and fire disturbance submodules [*Liu et al*., 2013; *Tian et al*., 2015; *Ren et al*., 2015; *Tao et al*., 2014; *Yang et al*., 2014a, 2015].

2.2.1. Parameterization of Pyrogenic Carbon Emissions

Similar to Global Fire Emissions Database (GFED3) [*van der Werf et al*., 2010], available fuel in the DLEM includes vegetation biomass (leaf and stem), litter, coarse woody debris, and peat. Specifically, leaf refers to foliage; stem includes bole, bark, and branches; litter includes dead leaf and fine woody debris (<7.6 cm in diameter); and coarse woody debris refers to dead roundwood > 7.6 cm in diameter [*Zhang et al*., 2010].

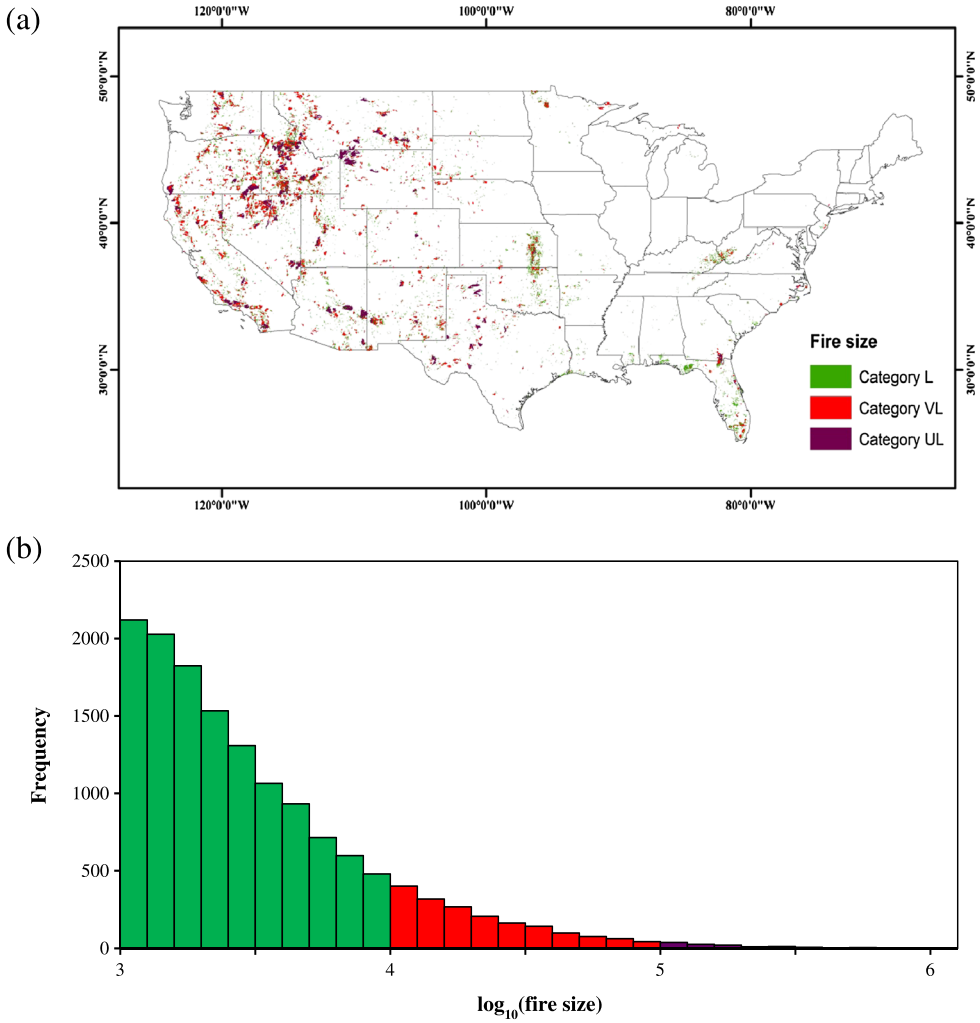

Figure 1. (a) Spatial distribution of fires by size category in conterminous United States and (b) the histogram of fire frequency in fire size intervals. The fire size intervals were created according to the logarithm of fire size (in acre).

However, the current version of DLEM did not explicitly simulated duff layer but treated duff layer as a part of soil carbon storage. Fuel loading is estimated according to a series of physiological processes (e.g., photosynthesis, respiration, and turnover) and biogeochemical processes (e.g., decomposition) (see the brief description in Text S2). The DLEM-simulated fuel loading has been validated against site level observations (such as Forest Inventory and Analysis plot data) in our previous studies [*Zhang et al.*, 2010; *Chen et al.*, 2013; *Tian et al.*, 2012]. In this study, we compared the DLEM-simulated vegetation carbon with the Intergovernmental Panel on Climate Change Tier-2 vegetation biomass data set at a national scale (Figure S2). The burned area and combustion completeness in the DLEM can either be obtained from input data or be simulated according to anthropogenic and environmental driving forces [*Yang et al.*, 2014a]. In this study, MTBS fire perimeter and burn severity data sets were incorporated into the DLEM to estimate pyrogenic carbon emissions (C_{bt}, g C m^{-2}),

$$C_{bt} = \sum_{ipft=1}^{4} \sum_{ifuel=1}^{4} \left(C_{ipft,\ ifuel}\ CC_{ipft,ifuel} BF_{ipft} f_{ipft} \right) \quad (2)$$

where ipft is the index of natural vegetation types within one model grid (DLEM allows a maximum of four natural vegetation types to coexist in one grid; see the major vegetation type in Figure S3); ifuel is the index of fuel types (1 = leaf, 2 = stem, 3 = litter, and 4 = coarse woody debris); BF_{ipft} is the monthly burned fraction of each natural vegetation type (%), which is assumed to be equal to burned fraction at grid level; f_{ipft} is the fraction of vegetation area; $C_{ipft,\ ifuel}$ is the DLEM-simulated fuel loading of each fuel types (g C m^{-2}); $CC_{ipft,ifuel}$

Table 1. Parameters of Combustion Completeness in Four Levels of Burn Severity ($CC_{ipft,ifuel,ibseve}$,%) Used in This Study

Vegetation	MTBS Burn Severity	Leaf	Stem	Litter	Coarse Woody Debris
Forest	Unburnt to low	3	1	57	26
	Low	31	10	64	35
	Moderate	54.5	45	64	42
	High	80	70	99	55
Shrub	Unburn to low	20	20	57	26
	Low	25	25	64	35
	Moderate	50	50	64	42
	High	95	95	99	55
Grass	Unburn to low	70	-	57	-
	Low	75	-	64	-
	Moderate	76	-	64	-
	High	100	-	99	-

is the combustion completeness (%), estimated according to the percentage of fire pixels in unburn to low, low, moderate, and high burn severity within one model grid (f_{ibseve}, %); and burn severity corresponded to combustion completeness ($CC_{ipft,ifuel,ibseve}$, %) in Table 1,

$$CC_{ipft,ifuel} = \sum_{ibseve=1}^{4} \left(f_{ibseve} CC_{ipft,ifuel,ibseve} \right) \quad (3)$$

where ibseve is the index of four burn severity levels. Combustion completeness in the DLEM is related to vegetation types, MTBS burn severity classes, and fuel types. The derivation of combustion completeness (%) from MTBS burn severity is illustrated in Table 1, which were compiled from some recent published literatures regarding burn severity in CONUS and across the globe [*Campbell et al*., 2007; *Ghimire et al*., 2012; *Liu et al*., 2011; *Meigs et al*., 2009; *van Leeuwen et al*., 2014].

It should be noted that the stem combustion completeness for moderate and high-severity fires is higher than field observations [*Campbell et al*., 2007; *Meigs et al*., 2009]. Based on Table 1, the effective stem combustion completeness is estimated to be 16.6% for fires in category L, 20.9% for fires in category VL, and 22.7% for fires in category UL, which falls within the range of stem combustion completeness used by large-scale land models [*van der werf et al*., 2010; *Li et al*., 2012; *Kloster et al*., 2010]. The discrepancy of stem combustion completeness between field observation and large-scale ecosystem models requires further investigation. The overestimation of fire emissions associated with higher stem combustion is offset to some extent by the absence of duff combustion.

2.2.2. Input Data to Drive the DLEM

In this study, the DLEM was run at a daily time step and a spatial resolution of 0.25° during 1979–2012. The pyrogenic carbon emissions were computed at a monthly time step. Georeferenced data sets driving the DLEM include daily climate data sets (downward solar radiation, precipitation, average/maximum/minimum temperature, and relative humidity), monthly burned fraction and burn severity, atmospheric CO_2 concentration, nitrogen deposition, land cover and land use, and soil texture and topography (elevation, slope, and aspect) for the entire CONUS. Climate conditions from 1979 to 2012 were derived from the NARR data set (see section 2.1.1). Time series of MTBS fire data were extracted from the fire perimeters according to fire start dates and then converted to fraction of burned area at the spatial resolution of 0.25°. For each grid, we estimated the percentages of burned area in unburn to low, low, moderate, and high burn severity levels based on the 30 m burn severity data (see example in Figure S1). When estimating the percentages of burn severity, satellite pixels labeled by increased greenness were merged into unburn to low severity group, and the pixels labeled by nonprocessing area mask were excluded. Other data sets (CO_2 concentration, nitrogen deposition, land use and land cover, soil texture, and topography) are consistent with our previous North America studies [*Liu et al*., 2013; *Yang et al*., 2014b].

2.2.3. Model Implementation

The implementation of the DLEM simulation is composed of three stages: equilibrium run, spin-up, and transient run. The equilibrium run aims to determine the initial status in the year 1979. During this stage, the DLEM was fed with the 10 year average climate conditions from 1979 to 1988, while other input data sets (atmospheric CO_2 concentration, nitrogen deposition, and land cover) were kept at the level of 1979. The

disturbances (such as fires, harvest, and land use change) were excluded in the equilibrium run. The equilibrium state for each grid cell was assumed to be reached when the differences in grid carbon, nitrogen, and water pools were less than 0.1 g C m^{-2}, 0.1 g N m^{-2}, and 0.1 mm between two consecutive 50 year periods. The equilibrium run was followed by a 100 year model spin-up. In the spin-up stage, the DLEM was driven by the detrended time series of all input data sets including fire disturbances. The detrended input data sets were constructed through random selection from the first 10 years (1979–1988). In the transient mode, the DLEM was driven by the time series of all the input data from 1979 to 2012. We simply assumed that fire conditions during 1979–1983 were the same as those in 1984 since the MTBS data records begin in 1984. We designed four experiments (*Sim0*, *Sim1*, *Sim2*, and *Sim3*) to investigate pyrogenic carbon emissions from large fires in different size categories. The reference simulation (*Sim0*) includes all the large fires with size over 1000 acres, while the other three simulation experiments include only fires in each size category, corresponding to fires in size category L, category VL, and category UL, respectively.

2.2.4. Evaluation of the DLEM-Simulated Pyrogenic Carbon Emissions

To evaluate the DLEM-simulated pyrogenic carbon emissions, we collected five fire products covering the entire CONUS, namely, Wildland Fire Emissions Information (WFEIS) v0.4 [*French et al.*, 2014], Global Fire Emissions Database (GFED) v3.1 [*van der Werf et al.*, 2010], Fire INventory from NCAR (FINN) v1 [*Wiedinmyer et al.*, 2011], Global Fire Assimilation System (GFAS) v1 [*Kaiser et al.*, 2012], and Geostationary Operation Environmental Satellites (GOES) [*Zhang et al.*, 2014] (see their availabilities in the supporting information). Year-to-year variation of the DLEM-simulated pyrogenic carbon emissions was compared with these fire products.

2.3. Statistical Analysis

The concept of characteristic fire size is designed to describe the relative contribution of fires in different sizes to the total burned area [*Lehsten et al.*, 2014]. The fire size with the largest contribution is defined as the characteristic fire size. We estimated the characteristic fire sizes in the entire study period (1984–2012) and three subperiods (1984–1993, 1994–2003, and 2004–2012), respectively. First, fires were separated into 20 bins with an equal width of logarithms of fire size (in acre). Then, unnormalized Gaussian curve (equation (4)) was used to fit the total burned area within each bin (dependent variable) against the midpoints of fire size in that bin (independent variable),

$$y = Ne^{-\frac{(x-\mu)^2}{2\sigma^2}} \tag{4}$$

where N is the height of the curve's peak, μ is the position of the peak, and σ is the standard deviation and controls the width of the Gaussian distribution. The three distribution parameters were acquired by using the least squares regression analysis. The fitted Gaussian curve is used to summarize the distribution of burned area against fire size, and the characteristic fire size is equal to 10^{μ} acres or $4.047 \times 10^{\mu-3}$ km^2.

The Mann-Kendall (MK) trend test is a nonparametric test to examine the trend significance of a time series. In this study, we applied the MK trend test to detect the significance of the trends in fire size, burned area, and fire-induced carbon emissions from 1984 to 2012. The slopes of annual burned area and fire-induced carbon emissions were estimated by using the least squares linear regression analysis.

3. Results and Discussion

3.1. Burned Area and Fire Size

From 1984 to 2012, there were 14,495 large fires included in MTBS across CONUS (Table S1), most of which occurred in the western U.S. (Figure 1a). Fire frequency decreases rapidly as fire size increases. The UL fires were only 0.81% of total fire numbers but accounted for 22.18% of the total burned area in CONUS (Figures 1b and 2a). During the study period, annual burned area derived from all the large fires was 14,431 ± 10,317 km^2 yr^{-1} (average ± 1 standard deviation, same hereafter) with a significant upward trend at the rate of 810 km^2 yr^{-1} ($P < 0.001$; Figure 3a). The highest annual burned area (40,474 km^2) was in 2011, while the lowest annual burned area (2499 km^2) was in 1997. Significant increasing trends were found for burned area in each of the three size categories (Table 2). Compared to the period of 1984–1993, annual burned area of all the large fires increased by 187.3% during 2004–2012, while the area burned by fires in category UL increased by 361.7%. Further analysis shows that the percent of area burned by category UL fires increased from 16.8% to 27%, while the percent of area burned by fires in category L decreased from 39.9% to 32.6% (Figure 3b).

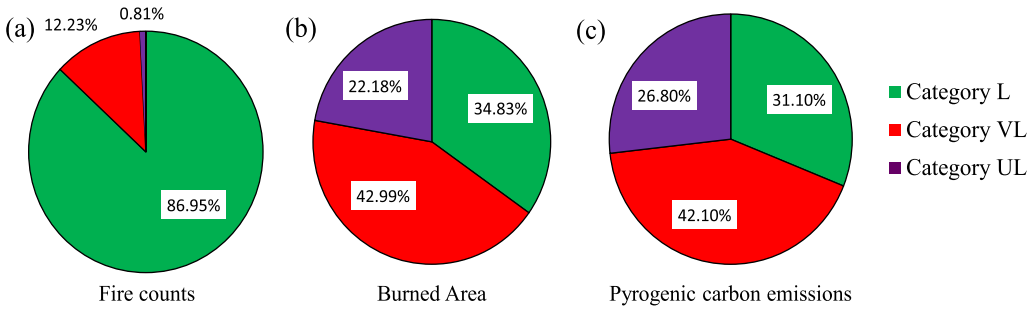

Figure 2. Contributions of fires by size category to (a) total fire counts, (b) total burned area, and (c) total pyrogenic carbon emissions in conterminous United States.

During 1984–2012, the characteristic fire size was estimated to be 80 km^2 (i.e., $10^{4.3}$ acres) (Figure 4). In the three subperiods of 1984–1993, 1994–2003, and 2004–2012, the characteristic fire sizes were estimated to be 48.3 km^2 (i.e., $10^{4.08}$ acres), 74.2 km^2 (i.e., $10^{4.26}$ acres), and 133.4 km^2 (i.e., $10^{4.52}$ acres), respectively. Compared to the first period (1984–1993), the characteristic fire size in the last period (2004–2012) increased by 176.1%. These results indicated that the size of fires with the maximum contribution to burned area was increasing over the recent three decades. Nevertheless, it is worth mentioning that no significant trend was found for the arithmetic annual mean of fire size from 1984 to 2012 ($P > 0.05$, Figure S4 in the supporting information) because burned area and fire frequencies increased simultaneously.

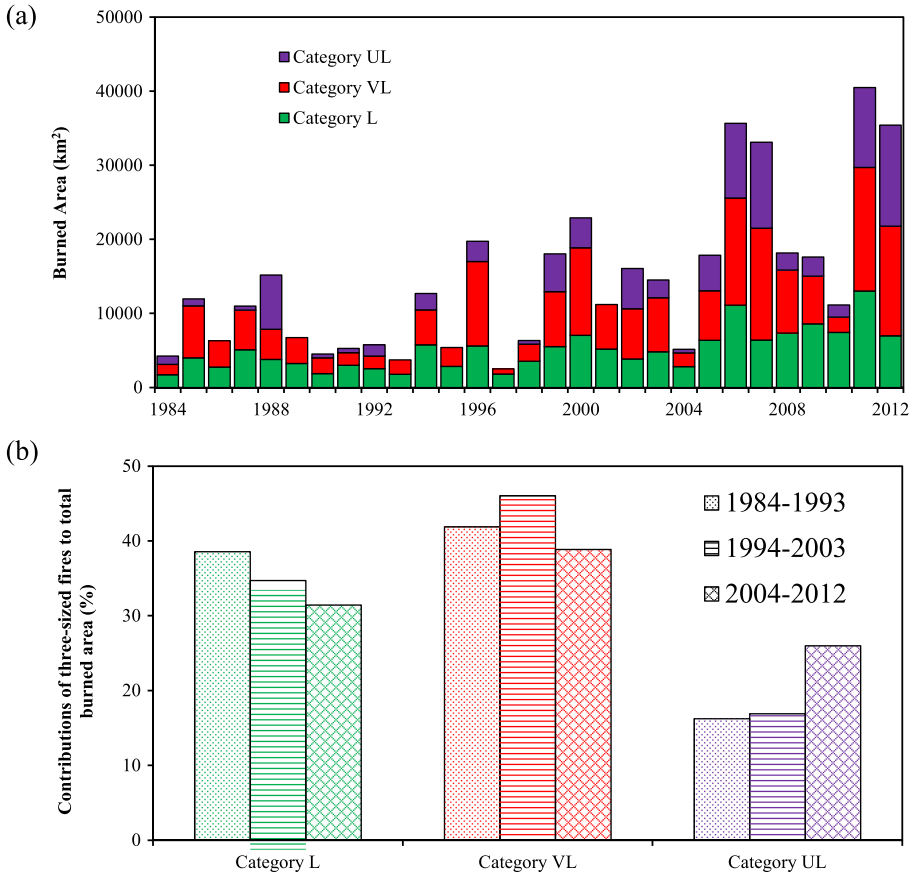

Figure 3. (a) Interannual variation of burned area in conterminous United States during 1984–2012 and (b) contributions of fires by size category to burned area during 1984–1993, 1994–2003, and 2004–2012.

Table 2. The Means and Trends of Burned Area and Pyrogenic Carbon Emissions in Conterminous United States

	Burned Area			Pyrogenic Carbon Emissions		
	Mean ($km^2\ yr^{-1}$)	Trend ($km^2\ yr^{-1}$)	*P* Value in MK Trend Test	Mean ($Tg\ C\ yr^{-1}$)	Trend ($Tg\ C\ yr^{-1}$)	*P* Value in MK Trend Test
All categories	14,430.51	810.29	<0.001	17.65	0.87	<0.01
Category L	5,026.01	231.30	<0.001	5.68	0.25	<0.001
Category VL	6,203.34	317.02	<0.01	7.7	0.39	<0.01
Category UL	3,201.16	261.97	<0.01	4.9	0.29	<0.01

3.2. Pyrogenic Carbon Emissions

During 1984–2012, annual pyrogenic carbon emissions from large fires were simulated to be 17.65 ± 12.68 $Tg\ C\ yr^{-1}$ with a significant increasing trend at the rate of 0.87 $Tg\ C\ yr^{-1}$ (Figure 5a and Table 2). The largest annual pyrogenic carbon emissions (48.11 Tg C) were in 2007, and the lowest pyrogenic carbon emissions (1.6 Tg C) were in 1984. Carbon emissions from UL fires accounted for 26.8% of the total carbon emissions from all the large fires (Figure 2). It should be noted that the sum of pyrogenic carbon emissions in *Sim1*, *Sim2*, and *Sim3* experiments was slightly higher than those estimated by *Sim0* experiment, although the sum of burned area in *Sim1*, *Sim2*, and *Sim3* was equal to that of *Sim0* (Figure 5a). This mismatch was primary because *Sim1*, *Sim2*, and *Sim3* only considered fires in single size category. Therefore, more fuel was accumulated in *Sim1*–*Sim3* than that in *Sim0*. Compared to the period of 1984–1993, mean annual carbon emissions from UL fires simulated by *Sim3* increased by 1.16 $Tg\ C\ yr^{-1}$ during 1994–2003 and increased by 5.55 $Tg\ C\ yr^{-1}$ during 2004–2012; the percent of UL fire-induced carbon emissions increased from 26.6% in the period of 1984–1993 to 29.6% in the latest period of 2004–2012 (Figure 5b). It can be concluded that the UL fires were becoming more important in term of fire emissions in recent decades. Between the period of 1984–1993 and the period of 2004–2012, the contribution of UL fires to burned area increased by 10.2 percentage points (see section 3.1), while contribution to carbon emissions only increased by 3 percentage points. This is possibly due to the high pyrogenic carbon emissions from UL fires in the period of 1984–1993, especially in 1988 when the UL fires emitted 21.8 Tg C to the atmosphere, equivalent to 66.4% of the total annual fire emissions.

The interannual variation of the DLEM-simulated pyrogenic carbon emissions was compared with other five fire emission products (Figure 6). The results indicated that the DLEM-simulated pyrogenic carbon emissions

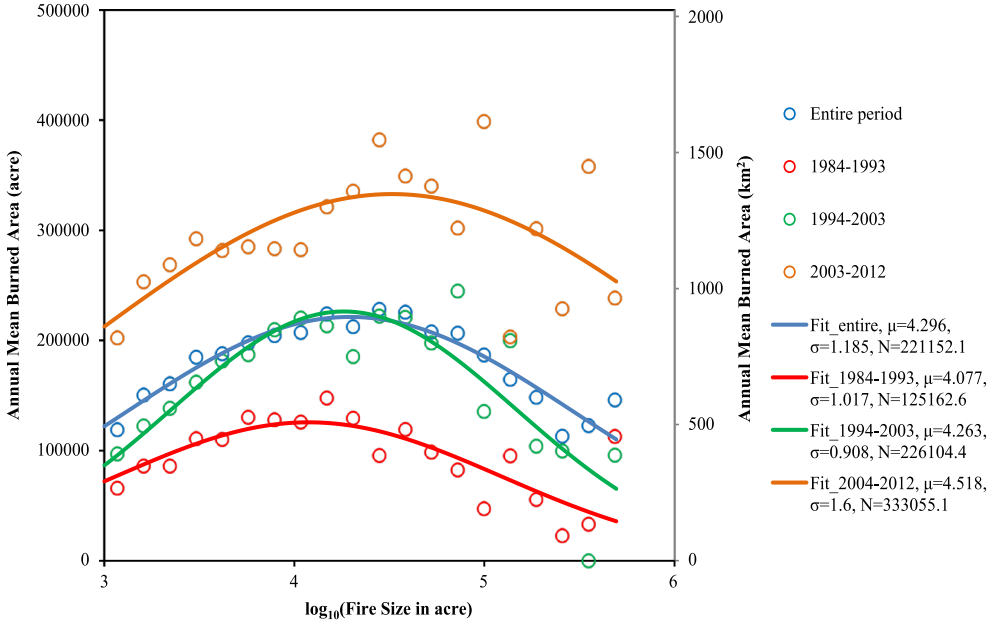

Figure 4. Characteristic fire size in the entire study period (1984–2012) and three subperiods (i.e., 1984–1993, 1994–2003, and 2004–2012). The plots were fitted with nonnormalized Gaussian distribution curve, and μ, σ and *N* in the legends are fitting parameters.

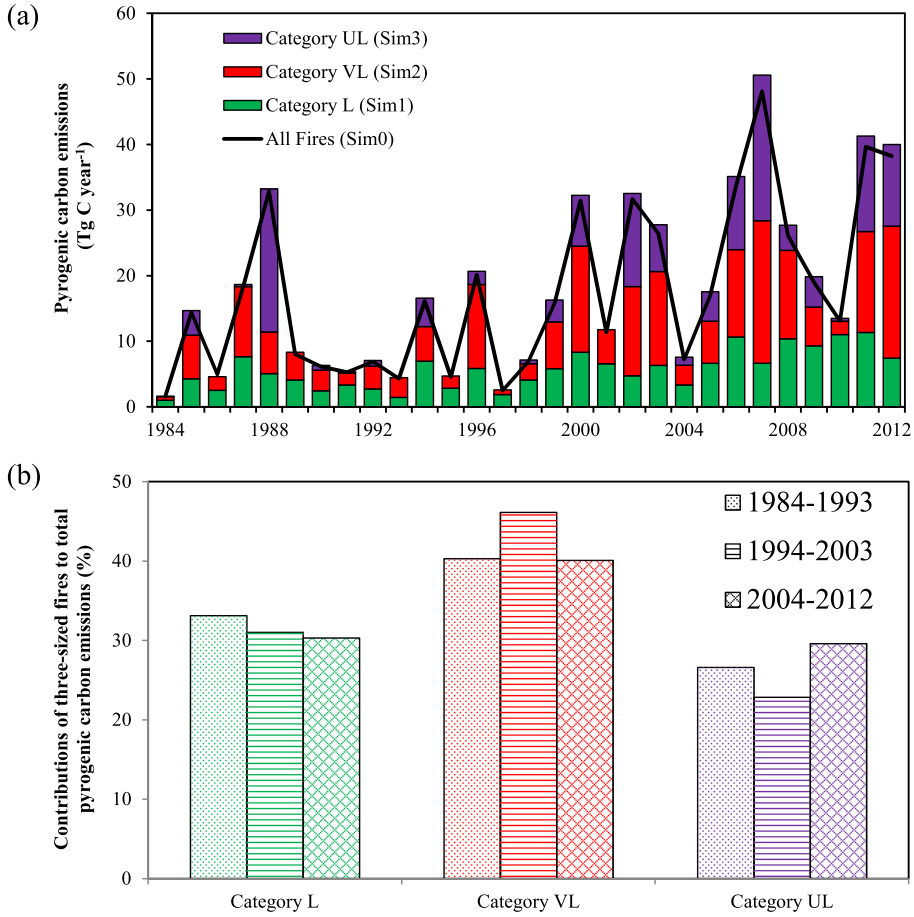

Figure 5. (a) Interannual variation of pyrogenic carbon emissions in conterminous United States during 1984–2012 and (b) contributions of fires by size category to pyrogenic carbon emissions during 1984–1993, 1994–2003, and 2004–2012, respectively.

were significantly correlated with each of the fire products (Table 3), which was partially due to the fact that all the fire products incorporated satellite information (either satellite-based burned area or FRP). During 2003–2010 (a period that all fire products covered), the DLEM-estimated mean annual pyrogenic carbon emissions were 23.8 Tg C yr^{-1}, which were close to the average of the other five fire products (26.1 Tg C yr^{-1}). However, GFED v3.1 pyrogenic carbon emissions were 69% lower than the average of the

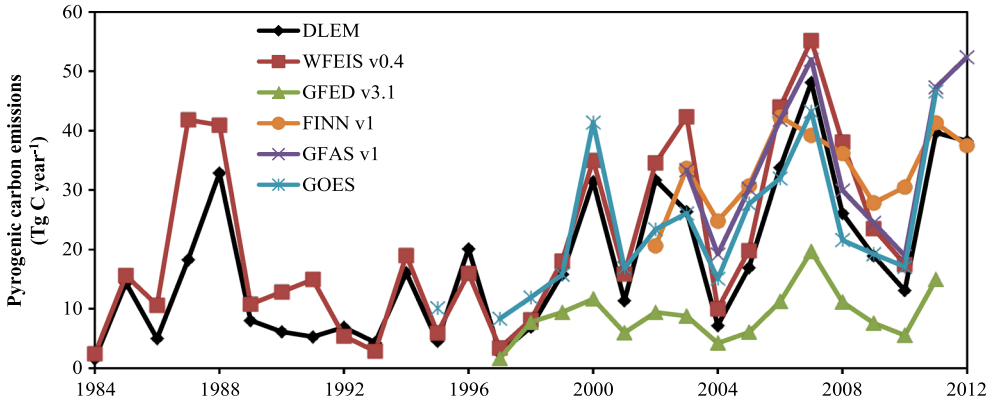

Figure 6. Intercomparison of annual pyrogenic carbon emissions in conterminous United States estimated by the DLEM, WFEIS v0.4, GFED v3.1, GFAS v1, GOES, and FINN v1.

Table 3. The Estimates of Pyrogenic Carbon Emissions Derived From Five Fire Emissions Products and Their Correlations With the DLEM Simulations (Values in the Parentheses Are Estimated by the DLEM)

Fire Products	Available Period	Pyrogenic Carbon Emissions (Tg C yr^{-1})	Pearson's Correlation Coefficient	Significance
WFEIS v0.4	1984–2010	20.9 (16.1)	0.94	$p < 0.001$
GFED v3.1	1997–2011	9 (22)	0.92	$p < 0.001$
FINN v1	2002–2012	33.2 (27.3)	0.66	$p < 0.05$
GFAS v1	2003–2012	35 (26.9)	0.95	$p < 0.001$
GOES	1995 and 1997–2011	23.5 (20.9)	0.91	$p < 0.001$

other five fire products. This is consistent with *Kaiser et al.* [2012] and *Zhang et al.* [2014], who argued that fire emissions estimated by GFED v3.1 were likely underestimated in CONUS. *Kasischke et al.* [2011] found a lower burned area estimate of GFED v3.1 than that reported by land management agencies, which may account for the lower pyrogenic carbon emissions in GFED v3.1.

Combustion completeness varies with locations, time periods, and climate conditions and is one of major uncertainties in the fire emissions estimation [*Yang et al.*, 2015]. Fire emission models using a set of combustion completeness parameters could overestimate/underestimate carbon emissions during fire events with extreme low/high severity. For example, as indicated by the MTBS data set, 45.3% of fire pixels within the North Fork fire perimeter were associated with high severity, which was much higher than the average burn severity in CONUS (on average, 8.64% of burned area was associated with high severity). Using a set of combustion completeness parameters could inevitably underestimate fire emissions caused by the North Fork fire. In this study, the DLEM considered the temporal and spatial variations of burned severity by incorporating satellite-derived burn severity data. This strategy enables the DLEM to better represent the large spatial and temporal variations in combustion completeness, particularly for the fires with a large portion of high burn severity.

3.3. Impacts of Climate and Fuel Loading on Large Fires

Fire spread rate and fire intensity are determined by the "fire behavior triangle," i.e., weather conditions, the amount and arrangement of fuel, and the topography. In this study, we focus on climate and fuel loading impacts on large fires. We examined fire frequency in four climate conditions, which are defined based on the *z* scores of annual temperature and precipitation: (i) dry and cool ($P_z < 0$ and $T_z < 0$), (ii) dry and warm ($P_z < 0$ and $T_z > 0$), (iii) wet and cool ($P_z > 0$ and $T_z < 0$), and (iv) wet and warm ($P_z > 0$ and $T_z > 0$). If fire occurrence is completely random, same possibilities of fire frequency are expected in the four climate conditions. However, the results showed that 44.8% of L fires, 49.3% of VL fires, and 59.3% of UL fires occurred in the relative dry and warm years ($P_z < 0$ and $T_z > 0$) (Figure 7), which is consistent with lower annual precipitation and higher annual temperatures facilitating large fire occurrences, particularly for the UL fires. This result is in line with previous literatures. *Westerling et al.* [2006] reported that the increases in wildfire activities in the western U.S. are associated with higher spring and summer temperature. *Dennison et al.* [2014] found that the regions in the western U.S. with most significant increases in fire activities are coincident with trends toward increased drought severity. *Riley et al.* [2013] found a strong correlation between fire activities and monthly precipitation in the western U.S. Combining these findings and our analysis, we can conclude that warm and dry climate condition is one factor controlling the increased frequency of large fires. It is noteworthy that decreased precipitation was also found to reduce the occurrence of large fires in some rangeland areas by suppressing vegetation growth and fuel accumulation [*Barbero et al.*, 2014].

In CONUS, contemporary burned area is approximately 2% of the level in the pre-European settlement era [*Houghton et al.*, 2000]. Annual burned area in California in the pre-European settlement is about 88% of the total burned area in CONUS in recent decades [*Stephens et al.*, 2007]. In the twentieth century, a large portion of fire activities were suppressed as a result of the fire exclusion policies in CONUS [*Houghton et al.*, 2000]. The Weeks Act of 1911 established a framework between the states and federal government for cooperative firefighting and was greatly extended with the Clark-McNary Act of 1924 and the McSweeney-McNary Act of 1928 [*Houghton et al.*, 2000]. The successful fire suppression policies promoted tree regeneration and fuel accumulation across all the forest types [*Agee and Skinner*, 2005]. The dense small trees filled the forest openings, increased the risk of crown fires, and facilitated fire spread. The

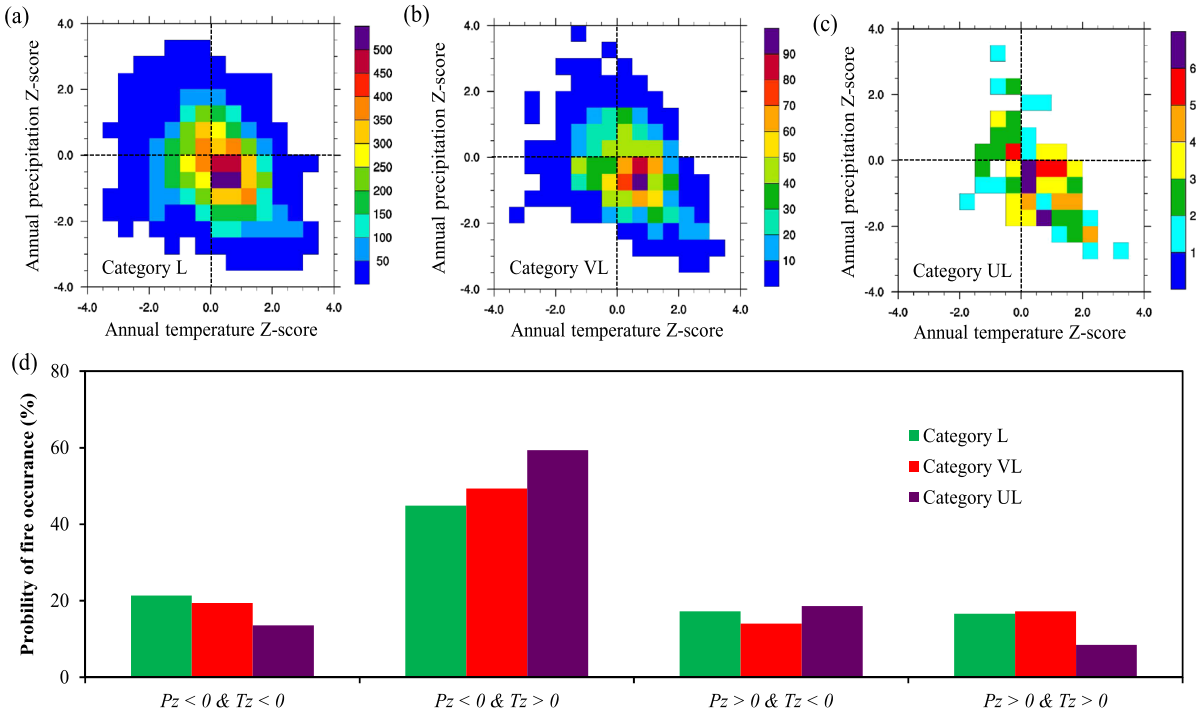

Figure 7. The plots of fire counts in size (a) category L, (b) category VL, and (c) category UL against the *z* scores of annual precipitation (*y* axis) and annual mean temperature (*x* axis). (d) The probability of fire occurrence in four climate conditions: (i) dry and cool ($P_z < 0$ and $T_z < 0$), (ii) dry and warm ($P_z < 0$ and $T_z > 0$), (iii) wet and cool ($P_z > 0$ and $T_z < 0$), and (iv) wet and warm ($P_z > 0$ and $T_z > 0$).

accumulation of surface fuel (such as litter and woody debris) increased fire intensity and flame length. Changes in fuelbed properties and vegetation structure resulting partially from fire suppression can facilitate fire spread and increase fire intensity, thereby contributing to the occurrence of large fires in the recent years [*Williams*, 2013].

3.4. The Relationship Between Fire Size and Burn Severity

Our results show that burn severity varies among different fire size categories. For the area burned by fires in categories L, VL, and UL, the percentages of "high severity" were 5.11%, 9.37%, and 12.84%, respectively (Figure 8). The sum of unburn to low and low severity was 79.3% for category L fires, comparing to 70% for category VL fires and 67.1% for category UL fires. These results indicated that fuel combustion completeness was lower for L fires than VL and UL fires, and fires in larger size were generally associated with higher burn severity in CONUS.

The general relationship between fire size and burn severity is a new finding and has not been investigated at a national scale in previous studies. At a smaller scale in northwestern California, *Miller et al*., 2012 reported that the proportion of area with high severity was related to the overall fire size by analyzing 132 MTBS fire records from 1987 to 2008. This is consistent with our results in spite of the different study domains. However, it should be pointed out that this general relationship was obtained based on the average condition of all the large fires in CONUS and may not be true for one specific fire event.

This relationship might be explained by the environmental factors that influence fire size and burn severity simultaneously. As we discussed above, fire size could be affected by changes in climate conditions and fuel loading. Meanwhile, climate and fuel loading also have strong influences on burn severity. For fires in extreme fire weather, more energy is released, and the surface fire more likely makes the transition to crown fire and leads to more severe consequences [*Dillon et al*., 2011]. Fire suppression activities in the twentieth century altered fuel status by promoting the establishment of small fire-intolerant trees under the forest canopy, which formed "ladder fuel" to carry the surface fire into the continuous canopy and enhanced the probability of catastrophic crown fires [*Schoennagel et al*., 2004]. The surface fuel accumulation enhanced fire intensity and caused more complete fuel consumption. Both fire size and burn severity are affected by

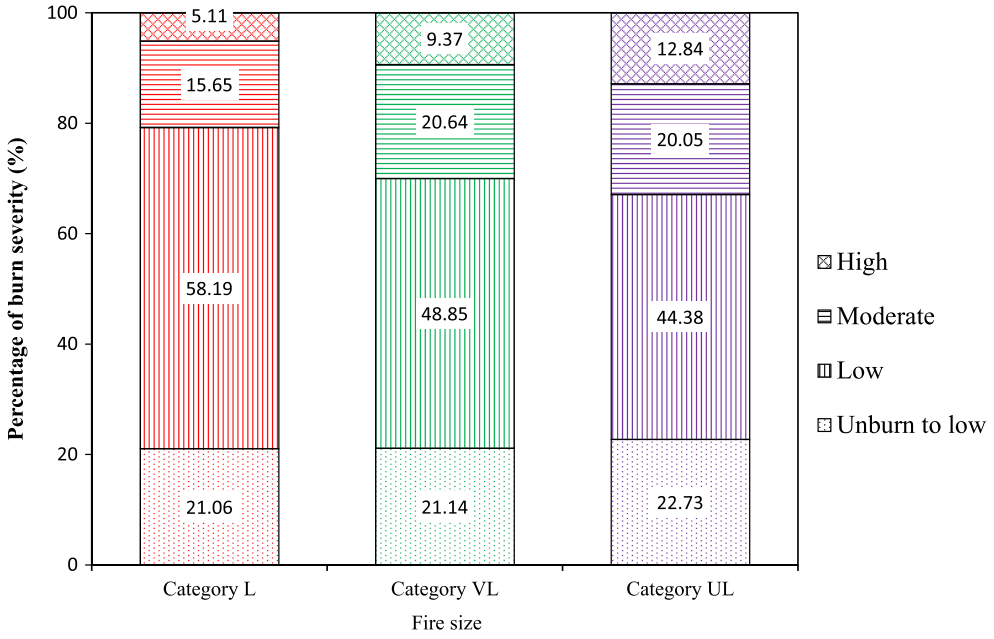

Figure 8. The burn severity (unburn to low, low, moderate, and high) distribution of burned pixels within three fire size categories.

climatic conditions and fuel loading, which explains the phenomenon that the larger fires are generally associated with higher burn severity in CONUS.

3.5. Uncertainties

Our study provided a practical approach for the ecosystem model to estimate large-scale fire emissions by incorporating satellite-based burn severity. This method might improve the accuracy of the model-based assessment of fire emissions. Nonetheless, uncertainties from both input data sets and model parameterizations should be beard in mind. First, in the MTBS, the threshold to classify burn severity in each satellite pixel is a quality control issue. Members of the mapping team discussed and designed feasible dNBR threshold for classifying burn severity under various environmental conditions (see the detailed processes in *Eidenshink et al*. [2007]). Therefore, subjectivities were inevitably introduced into the burn severity identification, and the MTBS classifications may suffer from some inconsistencies and unknown biases. When estimating burned area, we did not exclude unburned islands within fire perimeters, which might induce an overestimation in simulating fire emissions. However, it is difficult to provide an accurate estimation of the area of unburned islands at a national scale based on current available data sets. Second, the simulated fuel loading by the DLEM is another major source of uncertainty, although the simulated vegetation biomass has been validated against benchmarks. The DLEM simulates the average fuel loading at grid level by a series of physiological and biogeochemical processes (see Text S2 in the supporting information). Model parameterization affecting each of these processes contributed to the uncertainties in estimating fuel loading, fire emissions, and forest regrowth. Many disturbances, such as insect, tornado, and forest management, were not considered in this study, which might affect the accuracy of the DLEM-simulated fuel accumulation rate and fuel loading. Duff is an important component of surface fuel in CONUS [*Keane et al*., 2013]. However, it was not explicitly simulated by the DLEM. According to *Campbell et al*. [2007], the absence of duff combustion can cause an underestimation of about 30% of fire emissions. To accurately estimate fire emissions, there is a research need to address the fuel loading simulation by explicitly representing duff layer in ecosystem models. The assumption regarding the relationship between MTBS burn severity classes and fuel combustion (Table 1) is an important uncertainty source in simulating fire emissions. Third, scaling issue contributes another uncertainty source. To be compatible with the DLEM simulation, the 30 m MTBS burn severity was scaled up to 0.25°. Therefore, the subgrid variation in burn severity was neglected in the scaling-up process.

At the global scale, time series of dNBR have been developed based on Moderate Resolution Imaging Spectroradiometer data set [*Veraverbeke et al*., 2011]. The method to estimate fire emissions by integrating satellite-sensed burned severity should be used with caution when the study domain shifts to other regions. For example, in boreal regions, the relationship between dNBR and ground-based burn severity measurements has not been fully established. Some studies showed good relationship between dNBR and CBI [*Epting et al*., 2005; *Rogers et al*., 2014], while others found that their correlation is weak [*Hoy et al*., 2008; *Kasischke et al*., 2008; *Murphy et al*., 2008]. Prior to applying satellite-based burn severity, it is necessary to validate satellite-based burn severity indices against in situ measurement. In CONUS, a strong correlation was found between the dNBR and ground-based CBI [e.g., *Cocke et al*., 2005; *Key and Benson*, 2006; *Miller and Thode*, 2007; *Holden et al*., 2009; *Wimberly and Reilly*, 2007]. Therefore, burn severity derived from dNBR could be used in CONUS to quantify fire emissions [e.g., *Liu et al*., 2011; *Hicke et al*., 2013; *Campbell et al*., 2007; *Ghimire et al*., 2012].

4. Conclusions and Implications

In this study, we investigated the magnitude and changing trends of burned area and pyrogenic carbon emissions from large fires in conterminous United States during 1984–2012. We found that both burned area and pyrogenic carbon emissions presented significantly upward trends in the study period. The contributions of larger fires to total burned area and pyrogenic carbon emissions have been becoming higher in recent decades. We also found that the larger fires were generally associated with higher burn severity. This study provides the first attempt to couple a process-based land ecosystem model with combustion completeness estimates derived from high-resolution satellite burn severity for estimating pyrogenic carbon emissions over conterminous United States. The accuracy of model-simulated fire emission and fuel consumption in historical and contemporary periods can be improved by incorporating the remote-sensed spatiotemporal variations in burn severity.

Climate model projections indicate that the warming and drying trends would continue throughout the 21st century in conterminous United States, particularly under the high greenhouse gas emissions scenario [*Dai*, 2011; *Wuebbles et al*., 2014]. The increased temperature and drought will cause more fires and larger burned area in the future [*Westerling et al*., 2011; *Spracklen et al*., 2009]. According to our analysis that dry and warm conditions enhance the frequency of large fires (see section 3.3), it is rational to expect that the frequency of large fires will likely increase in the future, resulting in higher fuel combustion rate and more fire emissions. To obtain an accurate fire emission estimate, both burned area and fuel combustion completeness should be well represented by the process-based land ecosystem model. Further improvement in the parameterization of combustion completeness is required to reduce uncertainties in projecting future fire emissions.

Acknowledgments

This research has been supported by NSF/USDA/DOE Decadal and Regional Climate Prediction using Earth System Models (AGS-1243232, AGS-1243220, and NIFC2013-35100-20516), USDA/USDI Joint Fire Science Program (JFSP 11172), and NASA Carbon Monitoring System Project (NNX14AO73G). We appreciate the assistance of Brad Quayle at USDA Forest Service and Steve Howard at U.S. Geological Survey with MTBS data. We also thank the valuable and constructive comments from the three anonymous reviewers. The availability of MTBS fire data, climate data, and other driving forces is described in sections 3 and 6. The data sets to validate the model simulation are described in the supporting information.

References

Agee, J. K., and C. N. Skinner (2005), Basic principles of forest fuel reduction treatments, *For. Ecol. Manage.*, *211*(1), 83–96.

Barbero, R., J. Abatzoglou, E. A. Steel, and N. K. Larkin (2014), Modeling very large-fire occurrences over the continental United States from weather and climate forcing, *Environ. Res. Lett.*, *9*(12), 124,009.

Beck, P. S., S. J. Goetz, M. C. Mack, H. D. Alexander, Y. Jin, J. T. Randerson, and M. Loranty (2011), The impacts and implications of an intensifying fire regime on Alaskan boreal forest composition and albedo, *Global Change Biol.*, *17*(9), 2853–2866.

Bond, W., F. Woodward, and G. Midgley (2005), The global distribution of ecosystems in a world without fire, *New Phytol.*, *165*(2), 525–538.

Bond-Lamberty, B., S. D. Peckham, D. E. Ahl, and S. T. Gower (2007), Fire as the dominant driver of central Canadian boreal forest carbon balance, *Nature*, *450*(7166), 89–92.

Bond-Lamberty, B., S. D. Peckham, S. T. Gower, and B. E. Ewers (2009), Effects of fire on regional evapotranspiration in the central Canadian boreal forest, *Global Change Biol.*, *15*(5), 1242–1254.

Bousquet, P., P. Ciais, J. Miller, E. Dlugokencky, D. Hauglustaine, C. Prigent, G. Van der Werf, P. Peylin, E.-G. Brunke, and C. Carouge (2006), Contribution of anthropogenic and natural sources to atmospheric methane variability, *Nature*, *443*(7110), 439–443.

Bowman, D. M., J. K. Balch, P. Artaxo, W. J. Bond, J. M. Carlson, M. A. Cochrane, C. M. D'Antonio, R. S. DeFries, J. C. Doyle, and S. P. Harrison (2009), Fire in the Earth system, *Science*, *324*(5926), 481–484.

Brewer, C. K., J. C. Winne, R. L. Redmond, D. W. Opitz, and M. V. Mangrich (2005), Classifying and mapping wildfire severity: A comparison of methods, *Photogramm. Eng. Remote Sens.*, *71*(11), 1311–1320.

Campbell, J., D. Donato, D. Azuma, and B. Law (2007), Pyrogenic carbon emission from a large wildfire in Oregon, United States, *J. Geophys. Res.*, *112*, GO4014, doi:l0.1029/2007JG00045.

Chen, G., H. Tian, C. Huang, S. A. Prior, and S. Pan (2013), Integrating a process-based ecosystem model with Landsat imagery to assess impacts of forest disturbance on terrestrial carbon dynamics: Case studies in Alabama and Mississippi, *J. Geophys. Res. Biogeosci.*, *118*, 1208–1224, doi:10.1002/jgrg.20098.

Cocke, A. E., P. Z. Fulé, and J. E. Crouse (2005), Comparison of burn severity assessments using Differenced Normalized Burn Ratio and ground data, *Int. J. Wildland Fire*, *14*(2), 189–198.

Dai, A. (2011), Drought under global warming: A review, *WIREs Clim Change*, *2*(1), 45–65.
Dennison, P. E., S. C. Brewer, J. D. Arnold, and M. A. Moritz (2014), Large wildfire trends in the western United States, 1984–2011, *Geophys. Res. Lett.*, *41*, 2928–2933, doi:10.1002/2014GL059576.
Dillon, G. K., Z. A. Holden, P. Morgan, M. A. Crimmins, E. K. Heyerdahl, and C. H. Luce (2011), Both topography and climate affected forest and woodland burn severity in two regions of the western US, 1984 to 2006, *Ecosphere*, *2*(12), 130.
Dore, S., M. Montes-Helu, S. C. Hart, B. A. Hungate, G. W. Koch, J. B. Moon, A. J. Finkral, and T. E. Kolb (2012), Recovery of ponderosa pine ecosystem carbon and water fluxes from thinning and stand-replacing fire, *Global Change Biol.*, *18*(10), 3171–3185.
Eidenshink, J., B. Schwind, K. Brewer, Z.-L. Zhu, B. Quayle, and S. Howard (2007), A project for monitoring trends in burn severity, *Fire Ecol.*, *3*(1), 3–21.
Epting, J., D. Verbyla, and B. Sorbel (2005), Evaluation of remotely sensed indices for assessing burn severity in interior Alaska using Landsat TM and ETM+, *Remote Sens. Environ.*, *96*(3), 328–339.
French, N. H., D. McKenzie, T. Erickson, B. Koziol, M. Billmire, K. A. Endsley, N. K. Yager Scheinerman, L. Jenkins, M. E. Miller, and R. Ottmar (2014), Modeling regional-scale wildland fire emissions with the Wildland Fire Emissions Information System, *Earth Interact.*, *18*(16), 1–26, doi:10.1175/EI-D-14-0002.1.
Ghimire, B., C. A. Williams, G. J. Collatz, and M. Vanderhoof (2012), Fire-induced carbon emissions and regrowth uptake in western U.S. forests: Documenting variation across forest types, fire severity, and climate regions, *J. Geophys. Res.*, *117*, doi:10.1029/2011JG001935.
Hicke, J. A., A. J. Meddens, C. D. Allen, and C. A. Kolden (2013), Carbon stocks of trees killed by bark beetles and wildfire in the western United States, *Environ. Res. Lett.*, *8*(3), 035032.
Holden, Z., P. Morgan, and J. S. Evans (2009), A predictive model of burn severity based on 20-year satellite-inferred burn severity data in a large southwestern US wilderness area, *For. Ecol. Manage.*, *258*(11), 2399–2406.
Houghton, R., J. Hackler, and K. Lawrence (2000), Changes in terrestrial carbon storage in the United States. 2: The role of fire and fire management, *Global Ecol. Biogeogr.*, *9*(2), 145–170.
Hoy, E. E., N. H. French, M. R. Turetsky, S. N. Trigg, and E. S. Kasischke (2008), Evaluating the potential of Landsat TM/ETM+ imagery for assessing fire severity in Alaskan black spruce forests, *Int. J. Wildland Fire*, *17*(4), 500–514.
Kaiser, J., A. Heil, M. Andreae, A. Benedetti, N. Chubarova, L. Jones, J.-J. Morcrette, M. Razinger, M. Schultz, and M. Suttie (2012), Biomass burning emissions estimated with a global fire assimilation system based on observed fire radiative power, *Biogeosciences*, *9*(1), 527–554.
Kasischke, E. S., and M. R. Turetsky (2006), Recent changes in the fire regime across the North American boreal region—Spatial and temporal patterns of burning across Canada and Alaska, *Geophys. Res. Lett.*, *33*, L09703, doi:10.1029/2006GL025677.
Kasischke, E. S., E. J. Hyer, P. C. Novelli, L. P. Bruhwiler, N. H. French, A. I. Sukhinin, J. H. Hewson, and B. J. Stocks (2005), Influences of boreal fire emissions on Northern Hemisphere atmospheric carbon and carbon monoxide, *Global Biogeochem. Cycles*, *19*, GB1012, doi:10.1029/2004GB002300.
Kasischke, E. S., M. R. Turetsky, R. D. Ottmar, N. H. French, E. E. Hoy, and E. S. Kane (2008), Evaluation of the composite burn index for assessing fire severity in Alaskan black spruce forests, *Int. J. Wildland Fire*, *17*(4), 515–526.
Kasischke, E. S., T. Loboda, L. Giglio, N. H. French, E. E. Hoy, B. de Jong, and D. Riano (2011), Quantifying burned area for North American forests: Implications for direct reduction of carbon stocks, *J. Geophys. Res.*, *116*, G04003, doi:10.1029/2011JG001707.
Keane, R. E. (2013), Describing wildland surface fuel loading for fire management: A review of approaches, methods and systems, *Int. J. Wildland Fire*, *22*, 51–62.
Keeley, J. E. (2009), Fire intensity, fire severity and burn severity: A brief review and suggested usage, *Int. J. Wildland Fire*, *18*(1), 116–126.
Key, C. H., and N. C. Benson (2006), Landscape assessment (LA). FIREMON: Fire effects monitoring and inventory system Gen. Tech. Rep. RMRS-GTR-164-CD, Fort Collins, Colo: US Dep. of Agriculture, Forest Service, Rocky Mountain Research Station.
Kloster, S., N. M. Mahowald, J. T. Randerson, P. E. Thornton, F. M. Hoffman, S. Levis, P. J. Lawrence, J. J. Feddema, K. W. Oleson, and D. M. Lawrence (2010), Fire dynamics during the 20th century simulated by the Community Land Model, *Biogeosciences*, *7*, 1877–1902.
Langmann, B., B. Duncan, C. Textor, J. Trentmann, and G. R. van der Werf (2009), Vegetation fire emissions and their impact on air pollution and climate, *Atmos. Environ.*, *43*(1), 107–116.
Larkin, N. K., S. M. Raffuse, and T. M. Strand (2014), Wildland fire emissions, carbon, and climate: U.S. emissions inventories, *For. Ecol. Manage.*, *317*, 61–69.
Lehsten, V., W. J. Groot, M. Flannigan, C. George, P. Harmand, and H. Balzter (2014), Wildfires in boreal ecoregions: Evaluating the power law assumption and intra-annual and interannual variations, *J. Geophys. Res. Biogeosci.*, *119*, 14–23, doi:10.1002/2012JG002252.
Li, F., X. Zeng, and S. Levis (2012), A process-based fire parameterization of intermediate complexity in a Dynamic Global Vegetation Model, *Biogeosciences*, *9*(7), 2761–2780.
Li, F., B. Bond-Lamberty, and S. Levis (2014), Quantifying the role of fire in the Earth system—Part 2: Impact on the net carbon balance of global terrestrial ecosystems for the 20th century, *Biogeosciences*, *11*, 1345–1360.
Littell, J. S., D. McKenzie, D. L. Peterson, and A. L. Westerling (2009), Climate and wildfire area burned in western U.S. ecoprovinces, 1916–2003, *Ecol. Appl.*, *19*(4), 1003–1021.
Liu, J., et al. (2011), Estimating California ecosystem carbon change using process model and land cover disturbance data: 1951–2000, *Ecol. Modell.*, *222*(14), 2333–2341.
Liu, M., H. Tian, Q. Yang, J. Yang, X. Song, S. E. Lohrenz, and W. J. Cai (2013), Long-term trends in evapotranspiration and runoff over the drainage basins of the Gulf of Mexico during 1901–2008, *Water Resour. Res.*, *49*, 1988–2012, doi:10.1002/wrcr.20180.
Liu, Y. (2004), Variability of wildland fire emissions across the contiguous United States, *Atmos. Environ.*, *38*(21), 3489–3499.
Meigs, G. W., D. C. Donato, J. L. Campbell, J. G. Martin, and B. E. Law (2009), Forest fire impacts on carbon uptake, storage, and emission: The role of burn severity in the Eastern Cascades, Oregon, *Ecosystems*, *12*(8), 1246–1267.
Meigs, G. W., D. P. Turner, W. D. Ritts, Z. Yang, and B. E. Law (2011), Landscape-scale simulation of heterogeneous fire effects on pyrogenic carbon emissions, tree mortality, and net ecosystem production, *Ecosystems*, *14*(5), 758–775.
Mesinger, F., G. DiMego, E. Kalnay, K. Mitchell, P. C. Shafran, W. Ebisuzaki, D. Jović, J. Woollen, E. Rogers, and E. H. Berbery (2006), North American regional reanalysis, *Bull. Am. Meteorol. Soc.*, *87*(3), 343–360, doi:10.1175/BAMS-87-3-343.
Miller, J., and A. E. Thode (2007), Quantifying burn severity in a heterogeneous landscape with a relative version of the delta Normalized Burn Ratio (dNBR), *Remote Sens. Environ.*, *109*(1), 66–80.
Miller, J., C. Skinner, H. Safford, E. E. Knapp, and C. Ramirez (2012), Trends and causes of severity, size, and number of fires in northwestern California, USA, *Ecol. Appl.*, *22*(1), 184–203.
Murphy, K. A., J. H. Reynolds, and J. M. Koltun (2008), Evaluating the ability of the differenced Normalized Burn Ratio (dNBR) to predict ecologically significant burn severity in Alaskan boreal forests, *Int. J. Wildland Fire*, *17*(4), 490–499.

North, M. P., S. L. Stephens, B. M. Collins, J. K. Agee, G. Aplet, J. F. Franklin, and P. Z. Fulé (2015), Reform forest fire management, *Science*, *349*(6254), 1280–1281.

Pan, S., et al. (2014), Complex spatiotemporal responses of global terrestrial primary production to climate change and increasing atmospheric CO_2 in the 21st century, *PLoS One*, *9*(11) e112810, doi:10.1371/journal.pone.0112810.

Prentice, I., D. Kelley, P. Foster, P. Friedlingstein, S. Harrison, and P. Bartlein (2011), Modeling fire and the terrestrial carbon balance, *Global Biogeochem. Cycles*, *25*, GB3005, doi:10.1029/2010GB003906.

Randerson, J., H. Liu, M. Flanner, S. Chambers, Y. Jin, P. Hess, G. Pfister, M. Mack, K. Treseder, and L. Welp (2006), The impact of boreal forest fire on climate warming, *Science*, *314*(5802), 1130–1132.

Ren, W., H. Tian, B. Tao, Y. Huang, and S. Pan (2012), China's crop productivity and soil carbon storage as influenced by multifactor global change, *Global Change Biol.*, *18*(9), 2945–2957.

Ren, W., H. Tian, B. Tao, J. Yang, S. Pan, W.-J. Cai, S. E. Lohrenz, R. He, and C. S. Hopkinson (2015), Large increase in dissolved inorganic carbon flux from the Mississippi River to Gulf of Mexico due to climatic and anthropogenic changes over the 21st century, *J. Geophys. Res. Biogeosci.*, *120*, 724–736, doi:10.1002/2014JG002761.

Riley, K. L., J. T. Abatzoglou, I. C. Grenfell, A. E. Klene, and F. A. Heinsch (2013), The relationship of large fire occurrence with drought and fire danger indices in the western USA, 1984–2008: The role of temporal scale, *Int. J. Wildland Fire*, *22*(7), 894–909.

Rogers, B. M., S. Veraverbeke, G. Azzari, C. I. Czimczik, S. R. Holden, G. O. Mouteva, F. Sedano, K. K. Treseder, and J. T. Randerson (2014), Quantifying fire-wide carbon emissions in interior Alaska using field measurements and Landsat imagery, *J. Geophys. Res. Biogeosci.*, *119*, 1608–1629, doi:10.1002/2014JG002657.

Schoennagel, T., T. T. Veblen, and W. H. Romme (2004), The interaction of fire, fuels, and climate across Rocky Mountain forests, *BioScience*, *54*(7), 661–676.

Seiler, W., and P. J. Crutzen (1980), Estimates of gross and net fluxes of carbon between the biosphere and the atmosphere from biomass burning, *Clim. Change*, *2*(3), 207–247.

Spracklen, D. V., L. J. Mickley, J. A. Logan, R. C. Hudman, R. Yevich, M. D. Flannigan, and A. L. Westerling (2009), Impacts of climate change from 2000 to 2050 on wildfire activity and carbonaceous aerosol concentrations in the western United States, *J. Geophys. Res.*, *114*, D20301, doi:10.1029/2008JD010966.

Stephens, S. L., R. E. Martin, and N. E. Clinton (2007), Prehistoric fire area and emissions from California's forests, woodlands, shrublands, and grasslands, *For. Ecol. Manage.*, *251*(3), 205–216.

Tao, B., H. Tian, W. Ren, J. Yang, Q. Yang, R. He, W. Cai, and S. Lohrenz (2014), Increasing Mississippi river discharge throughout the 21st century influenced by changes in climate, land use, and atmospheric CO_2, *Geophys. Res. Lett.*, *41*, 4978–4986, doi:10.1002/2014GL060361.

Thonicke, K., A. Spessa, I. Prentice, S. Harrison, L. Dong, and C. Carmona-Moreno (2010), The influence of vegetation, fire spread and fire behaviour on biomass burning and trace gas emissions: Results from a process-based model, *Biogeosciences*, *7*(6), 1991–2011.

Tian, H., X. Xu, M. Liu, W. Ren, C. Zhang, G. Chen, and C. Lu (2010a), Spatial and temporal patterns of CH_4 and N_2O fluxes in terrestrial ecosystems of North America during 1979–2008: Application of a global biogeochemistry model, *Biogeosciences*, *7*(9), 2673–2694, doi:10.5194/bg-7-2673-2010.

Tian, H., G. Chen, M. Liu, C. Zhang, G. Sun, C. Lu, X. Xu, W. Ren, S. Pan, and A. Chappelka (2010b), Model estimates of ecosystem net primary productivity, evapotranspiration, and water use efficiency in the Southern United States during 1895–2007, *For. Ecol. Manage.*, *259*(7), 1311–1327.

Tian, H., et al. (2012), Century-scale response of ecosystem carbon storage and flux to multifactorial global change in the Southern United States, *Ecosystems*, *15*(4), 674–694, doi:10.1007/s10021-012-9539-x.

Tian, H., Q. Yang, R. G. Najjar, W. Ren, M. A. M. Friedrichs, C. S. Hopkinson, and S. Pan (2015), Anthropogenic and climatic influences on carbon fluxes from eastern North America to the Atlantic Ocean: A process-based modeling study, *J. Geophys. Res. Biogeosci.*, *120*, 757–772, doi:10.1002/2014JG002760.

Urbanski, S. P., W. M. Hao, and B. Nordgren (2011), The wildland fire emission inventory: Western United States emission estimates and an evaluation of uncertainty, *Atmos. Chem. Phys.*, *11*(24), 12,973–13,000.

van der Werf, G. R., J. T. Randerson, G. J. Collatz, L. Giglio, P. S. Kasibhatla, A. F. Arellano, S. C. Olsen, and E. S. Kasischke (2004), Continental-scale partitioning of fire emissions during the 1997 to 2001 El Niño/La Niña period, *Science*, *303*(5654), 73–76.

van der Werf, G. R., J. T. Randerson, L. Giglio, G. Collatz, M. Mu, P. S. Kasibhatla, D. C. Morton, R. DeFries, Y. V. Jin, and T. T. van Leeuwen (2010), Global fire emissions and the contribution of deforestation, savanna, forest, agricultural, and peat fires (1997–2009), *Atmos. Chem. Phys.*, *10*(23), 11,707–11,735.

van Leeuwen, T. T., et al. (2014), Biomass burning fuel consumption rates: A field measurement database, *Biogeosci. Discuss.*, *11*(6), 8115–8180, doi:10.5194/bgd-11-8115-2014.

Veraverbeke, S., S. Lhermitte, W. W. Verstraeten, and R. Goossens (2011), A time-integrated MODIS burn severity assessment using the multi-temporal differenced normalized burn ratio ($dNBR_{MT}$), *Int. J. Appl. Earth Observ. Geoinform.*, *13*(1), 52–58.

Veraverbeke, S., B. M. Rogers, and J. T. Randerson (2015), Daily burned area and carbon emissions from boreal fires in Alaska, *Biogeosciences*, *12*(11), 3579–3601.

Ward, D., S. Kloster, N. Mahowald, B. Rogers, J. Randerson, and P. Hess (2012), The changing radiative forcing of fires: Global model estimates for past, present and future, *Atmos. Chem. Phys.*, *12*(22), 10,857–10,886.

Westerling, A., H. G. Hidalgo, D. R. Cayan, and T. W. Swetnam (2006), Warming and earlier spring increase western U.S. forest wildfire activity, *Science*, *313*(5789), 940–943.

Westerling, A., M. G. Turner, E. A. Smithwick, W. H. Romme, and M. G. Ryan (2011), Continued warming could transform Greater Yellowstone fire regimes by mid-21st century, *Proc. Natl. Acad. Sci. U.S.A.*, *108*(32), 13,165–13,170.

Wiedinmyer, C., S. K. Akagi, R. J. Yokelson, L. K. Emmons, J. A. Al-Saadi, J. J. Orlando, and A. J. Soja (2011), The Fire INventory from NCAR (FINN): A high resolution global model to estimate the emissions from open burning, *Geosci. Model Dev.*, *4*(3), 625–641, doi:10.5194/gmd-4-625-2011.

Williams, J. (2013), Exploring the onset of high-impact mega-fires through a forest land management prism, *For. Ecol. Manage.*, *294*, 4–10.

Wimberly, M., and M. J. Reilly (2007), Assessment of fire severity and species diversity in the southern Appalachians using Landsat TM and ETM+ imagery, *Remote Sens. Environ.*, *108*(2), 189–197.

Wooster, M. J., G. Roberts, G. Perry, and Y. Kaufman (2005), Retrieval of biomass combustion rates and totals from fire radiative power observations: FRP derivation and calibration relationships between biomass consumption and fire radiative energy release, *J. Geophys. Res.*, *110*, D24311, doi:10.1029/2005JD006318.

Wuebbles, D., G. Meehl, K. Hayhoe, T. R. Karl, K. Kunkel, B. Santer, M. Wehner, B. Colle, E. M. Fischer, and R. Fu (2014), CMIP5 climate model analyses: Climate extremes in the United States, *Bull. Am. Meteorol. Soc.*, *95*(4), 571–583.

Yang, J., H. Tian, B. Tao, W. Ren, J. Kush, Y. Liu, and Y. Wang (2014a), Spatial and temporal patterns of global burned area in response to anthropogenic and environmental factors: Reconstructing global fire history for the 20th and early 21st centuries, *J. Geophys. Res. Biogeosci.*, *119*, 249–263, doi:10.1002/2013JG002532.

Yang, J., H. Tian, B. Tao, W. Ren, C. Lu, S. Pan, Y. Wang, and Y. Liu (2015), Century-scale patterns and trends of global pyrogenic carbon emissions and fire impacts on the terrestrial carbon balance, *Global Biogeochem. Cycles*, *29*, 1549–1566, doi:10.1002/2015GB005160.

Yang, Q., H. Tian, X. Li, B. Tao, W. Ren, G. Chen, C. Lu, J. Yang, S. Pan, and K. Banger (2014b), Spatiotemporal patterns of evapotranspiration along the North American east coast as influenced by multiple environmental changes, *Ecohydrology*, *8*, 712–723, doi:10.1002/eco.1538.

Zhang, C., H. Tian, Y. Wang, T. Zeng, and Y. Liu (2010), Predicting response of fuel load to future changes in climate and atmospheric composition in the Southern United States, *For. Ecol. Manage.*, *260*(4), 556–564.

Zhang, X., S. Kondragunta, and D. P. Roy (2014), Interannual variation in biomass burning and fire seasonality derived from Geostationary satellite data across the contiguous United States from 1995 to 2011, *J. Geophys. Res. Biogeosci.*, *119*, 1147–1162, doi:10.1002/2013JG002518.